



Involvement of advillin in somatosensory neuron subtype-specific axon regeneration and neuropathic pain

Yu-Chia Chuang^{a,b,c}, Cheng-Han Lee^b, Wei-Hsin Sun^d, and Chih-Cheng Chen^{a,b,e,1}

^aTaiwan International Graduate Program in Molecular Medicine, National Yang-Ming University and Academia Sinica, 112 Taipei, Taiwan; ^bInstitute of Biomedical Sciences, Academia Sinica, 115 Taipei, Taiwan; ^cInstitute of Biochemistry and Molecular Biology, National Yang-Ming University, 112 Taipei, Taiwan; ^dDepartment of Life Sciences, National Central University, Zhongli, 32054 Taoyuan City, Taiwan; and ^eTaiwan Mouse Clinic–National Comprehensive Mouse Phenotyping and Drug Testing Center, Academia Sinica, 115 Taipei, Taiwan

Edited by Tomas Hökfelt, Karolinska Institutet, Stockholm, Sweden, and approved July 25, 2018 (received for review September 21, 2017)

Advillin is a sensory neuron-specific actin-binding protein expressed at high levels in all types of somatosensory neurons in early development. However, the precise role of advillin in adulthood is largely unknown. Here we reveal advillin expression restricted to isolectin B4-positive (IB4⁺) neurons in the adult dorsal root ganglia (DRG). Advillin knockout (KO) specifically impaired axonal regeneration in adult IB4⁺ DRG neurons. During axon regeneration, advillin was expressed at the very tips of filopodia and modulated growth cone formation by interacting with and regulating focal-adhesion-related proteins. The advillin-containing focal-adhesion protein complex was shed from neurite tips during neurite retraction and was detectable in cerebrospinal fluid in experimental autoimmune encephalomyelitis, oxaliplatin-induced peripheral neuropathy, and chronic constriction injury of the sciatic nerve. In addition, advillin KO disturbed experimental autoimmune encephalomyelitis-induced neural plasticity in the spinal-cord dorsal horn and aggravated neuropathic pain. Our study highlights a role for advillin in growth cone formation, axon regeneration, and neuropathic pain associated with IB4⁺ DRG neurons in adulthood.

advillin | CCI | EAE | IB4 | oxaliplatin

Neuropathic pain is characterized as a hypersensitive response to noxious and innocuous stimuli that result from a disease or lesion of the somatosensory nervous system at the peripheral or central level (1–3). Patients with chronic neuropathic pain experience daily pain that greatly impairs their quality of life. Because neuropathic pain is often difficult to treat (4), a proper diagnosis to demonstrate the cause of lesions is still essential for effective treatment (5).

In diabetic patients, neuropathic pain is accompanied by progressive loss of sensory nerve fibers and increased axonal regeneration in the epidermis (6, 7). Accumulating evidence has shown that proteins associated with the axonal regeneration program (e.g., axonal growth and cytoskeletal components, growth factors, neurotransmitter systems, and ion channels) are involved in the development of neuropathic pain (8). Although the relation between nerve regeneration and neuropathic pain is poorly understood and needs further investigation, the delivery of neurotrophic growth factors to enhance and guide axonal regeneration has been explored to treat pain associated with peripheral neuropathy (9).

Somatosensory neurons are composed of heterogeneous subtypes, including myelinated large-diameter neurons and nonmyelinated small-diameter neurons that can be further divided into peptidergic neurons containing the neuropeptide calcitonin gene-related peptide (CGRP) and/or substance P (SP) and non-peptidergic neurons that bind to isolectin B4 (IB4) (10). Different subtypes of somatosensory neurons have distinct intrinsic growth capacity and show heterogeneous responses to regeneration-promoting stimuli (11–14). IB4⁺ neurons have poor intrinsic axonal regeneration capacity compared with myelinated neurons (11, 15), whereas CGRP⁺ and myelinated dorsal root ganglia (DRG)

neurons show regenerative axons sprouting into spinal laminae after peripheral nerve injury (11). Nevertheless, the association between subtype-dependent nerve regeneration and neuropathic pain is poorly understood and needs further investigation.

Advillin is a sensory neuron-specific protein expressed in all types of somatosensory neurons (16, 17). Advillin-Cre knockin (*Avil^{+/cre}*) mice are well used for distinguishing the role of neuronal proteins in the central and peripheral system (18, 19). The exact function of advillin has not been well investigated, although its tissue distribution and expression during development have been finely scrutinized (18). Advillin interacts with β -actin (17) and the scavenger receptor SREC-I (20) and contributes to neurite outgrowth in vitro (17, 18). Advillin-knockout (KO) mice have no obvious phenotype in the normal physiological context but show impaired regenerative axon growth (18). From study of the homolog protein villin, advillin, belonging to the gelsolin superfamily, is assumed to regulate actin filament and modulate cytoskeletal dynamics (21). Advillin shares the conserved domain of villin that can both polymerize and depolymerize actin filaments depending on calcium concentration (21).

Surprisingly, previous genetic studies show no effect of advillin KO on axon growth and projection patterns of sensory neurons during prenatal development. Instead, advillin is involved in regenerative axon outgrowth in early postnatal stages (18). However, little is known about the expression and dynamic distribution of

Significance

An estimated 20 million people in the United States have chronic neuropathic pain, but current analgesics are nonspecific or insufficiently effective. Here we show that advillin, a sensory neuron-specific protein, modulates axonal regeneration of a specific subset of pain-sensing afferent neurons (nociceptors) that binds with isolectin B4 and neuropathic pain. In addition, we identify the cell behavior of advillin shed-off from the growth cone in the context of axonal regeneration and thus detected advillin protein in the cerebrospinal fluid in mice with painful peripheral neuropathy. Advillin is a potential biosignature to diagnose the lesion cause of neuropathic pain associated with isolectin B4⁺ nociceptors.

Author contributions: Y.-C.C., C.-H.L., W.-H.S., and C.-C.C. designed research; Y.-C.C. and C.-H.L. performed research; W.-H.S. contributed new reagents/analytic tools; Y.-C.C., C.-H.L., and C.-C.C. analyzed data; and Y.-C.C., W.-H.S., and C.-C.C. wrote the paper.

The authors declare no conflict of interest.

This article is a PNAS Direct Submission.

This open access article is distributed under [Creative Commons Attribution-NonCommercial-NoDerivatives License 4.0 \(CC BY-NC-ND\)](https://creativecommons.org/licenses/by-nc-nd/4.0/).

¹To whom correspondence should be addressed. Email: chih@ibms.sinica.edu.tw.

This article contains supporting information online at www.pnas.org/lookup/suppl/doi:10.1073/pnas.1716470115/-DCSupplemental.

Published online August 20, 2018.

advillin protein in living sensory neurons. Furthermore, whether advillin is involved in neural plasticity in adulthood, especially in the context of sensory neuropathy, is still not known.

Here, we used immunostaining, live imaging, biochemistry, and genetic approaches to examine the expression of advillin in axonal growth cones, the key structure that determines the destiny of neurite outgrowth. Then, we probed the roles of advillin in the context of nerve regeneration and neuropathic pain in: (i) a mouse model of multiple sclerosis induced by experimental autoimmune encephalomyelitis (EAE), a demyelinating autoimmune disease accompanied by severe sensory neuropathy (22, 23); (ii) a peripheral neuropathy model induced by oxaliplatin, a drug used to treat colorectal cancer (24); and (iii) a localized nerve lesion model induced by chronic constriction injury (CCI) of the sciatic nerve (25, 26).

Results

Characterization of Advillin Expression in DRG with Advillin-Specific Antibodies. To probe the expression and subcellular distribution of advillin protein in sensory neurons, we first generated specific antibodies for advillin based on a peptide antigen corresponding to the headpiece domain of advillin, as described previously (20). We validated the specificity of advillin antibodies in advillin-KO (*Avil*^{-/-}) mice. On Western blot analysis, the antibody detected a predicted 92-kDa protein in WT (WT or *Avil*^{+/+}) but not *Avil*^{-/-} DRG (*SI Appendix, Fig. S1A*). Villin, a functionally related protein of the gelsolin superfamily, was not detectable in *Avil*^{+/+} or *Avil*^{-/-} DRG, which indicates no obvious compensation. Advillin protein was not detectable in the intestine or cortex (*SI Appendix, Fig. S1A and B*), as reported previously (18). Advillin protein was detected in both the membrane fraction and cytosol of WT DRG (*SI Appendix, Fig. S1C*). Coimmunoprecipitation (Co-IP) of advillin antibody with DRG lysates showed an interaction between advillin and proteins at about 200 kDa (*SI Appendix, Fig. S1D*). LC-MS/MS analysis confirmed the major IP product containing advillin and uncovered nonmuscle myosin IIa (myosin 9, NP_071855) in the 200-kDa IP products, validated by myosin IIa-specific antibody (*SI Appendix, Fig. S1E*). Myosin IIa and advillin were not detectable in rabbit IgG IP products with corresponding sizes. Consistent with results of a heterologous cell expression system (17), advillin and actin interacted in DRG lysates (*SI Appendix, Fig. S1E*).

Advillin Protein Predominant in a Specific Subset of Adult DRG Neurons. As reported previously (18), advillin mRNA is expressed in all neuronal cells in DRG by mouse embryonic day 16.5 and its expression could last into postnatal stages. Moreover, a genetic-knockin approach revealed advillin expression in almost all types of sensory neurons. However, how advillin proteins are expressed and distributed in DRG neurons, especially in adulthood, is largely unknown. Here we found that, consistent with the previous report, advillin protein was expressed in most DRG neurons, and their central projection ranged from superficial layers to medial parts of the spinal cord in neonatal (P0) mice (*SI Appendix, Fig. S2 A and B*). Nevertheless, advillin immunoreactivity was detected in specific subsets of DRG neurons in adult mice (Fig. 1 *A and B*). In adult DRG, advillin was immunoreactive in ~40% of DRG neurons (2,256 of 5,095 from five mice), predominant in small-diameter nonpeptidergic (i.e., IB4⁺ neurons) and only partially overlapped with small-diameter peptidergic neurons that express CGRP and large-diameter neurons that express neurofilament-200 (N52⁺), with topology corresponding to their central projection to superficial layers of the spinal-cord dorsal horn (Fig. 1*C*) and peripheral projection to epidermal skin (Fig. 1*D*). Advillin was expressed in 85.2% (580 of 692) of IB4⁺, 17.1% (92 of 546) of CGRP⁺, and 19.2% (229 of 1,169) of N52⁺ DRG neurons (Fig. 1*B and SI Appendix, Table S1*). Advillin antibodies showed no obvious background staining in null mouse tissues, including the DRG, spinal cord, and skin (*SI Appendix, Fig. S2 C–E*). In the adult spinal dorsal horn, the

expression of advillin was expanded through superficial dorsal laminae (predominantly lamina I and II), colocalized with IB4 (62.6 ± 1.2%, in 61 z-section images), and overlapped with CGRP to a much lesser extent (15.2 ± 0.9%, in 51 z-section images) (Fig. 1 *C' and E*). The advillin-immunoreactivity pattern in the spinal-cord dorsal horn was in good agreement with the advillin expression profile in *Avil*^{+/Cre} mice (*SI Appendix, Fig. S3 A and B*), more confined in lamina II.

Subcellular Distribution and Functional Implication of Advillin in Sensory Terminals. Previous studies have shown a role for advillin in neurite outgrowth in vitro and axon regeneration in vivo (17, 18). Nevertheless, the precise role of advillin in coordinating neurite outgrowth is still unknown. To understand the precise role in neurite outgrowth, we analyzed the subcellular distribution of advillin in DRG nerve terminals. In cultured DRG neurons, advillin was immunoreactive along the soma to neurite shafts and even expanded to shaft filopodia and terminals that showed no β-tubulin III expression (Fig. 2*A*). Advillin was expressed in lamellipodia (Fig. 2*B'*, arrow) and filopodia (Fig. 2*B'*, arrowheads) of growth cones and colocalized with actin filaments (F-actin) (Fig. 2*B'*), whose subcellular distribution agrees with the presumed function of advillin modulating the actin dynamics of growth cones (27). In growth cones, 92.5 ± 1.4% of filopodia showed colocalization of advillin immunoreactivity with F-actin; 10.6 ± 2.3% of filopodia tips showed only advillin without F-actin (in 151 growth cones, 1,301 filopodia, 3 mice). The expression of advillin in axon terminals was further validated in the spinal-cord dorsal horn in *Avil*^{+/Cre}::*GFP* mice. In the same afferents in lamina II, the advillin immunoreactivity signal could reach the axon tips, where there was no GFP signal (*SI Appendix, Fig. S3C*). In vitro, all GFP⁺ cultured DRG neurons showed advillin immunoreactivity. However, only advillin immunoreactivity was observed in axon tips, especially in the growth cone area (*SI Appendix, Fig. S3 D and D'*).

To further probe the role of advillin in growth cones, we overexpressed advillin in a neural differentiation model of the Neuro-2a (N2a) cells. Under the undifferentiated condition, cells transfected with advillin showed multiple filopodia-like protrusions that were barely observed in cells transfected with GFP (*SI Appendix, Fig. S4A*). After retinoic acid-induced differentiation, cells with advillin overexpression showed increased process number and prolonged neurite length (*SI Appendix, Fig. S4A*). Advillin overexpression significantly increased the proportion of cells with multiple filopodia in the undifferentiated state and cells with neurites in the differentiated state (*SI Appendix, Fig. S4B*).

We next examined the real-time dynamics of advillin protein during neurite outgrowth. Time-lapse images were used to record N2a cells transfected with LifeAct-tagRFP, used to label F-actin, and GFP-advillin. Live imaging revealed a dynamic interaction between advillin and F-actin. Most importantly, advillin was expressed along the neurite shafts to the tips of active growth cones, dynamically interacting with F-actin during the neurite processing and regulating neurite retraction and formation of growth cones (Fig. 2*C* and *Movie S1*). In addition, before filopodia maturation, advillin appeared at the tips of newly forming filopodia, and F-actin followed behind as the filopodia elongated (Fig. 2*D*). Hence, advillin expression is closely associated with filopodia tips in active growth cones, which suggests that it could modulate neurite extension, retraction, and pathfinding via its dynamic interaction with F-actin.

Advillin Regulates Pathfinding During Axonal Outgrowth. We next probed whether advillin KO could affect axon regeneration of adult DRG neurons in vitro. Indeed, advillin KO reduced neurite length and decreased neurite branching (*SI Appendix, Fig. S5*). In contrast, advillin overexpression boosted filopodia formation and neurite branching (*Movie S2*) compared with normal advillin expression (*Movie S3*).

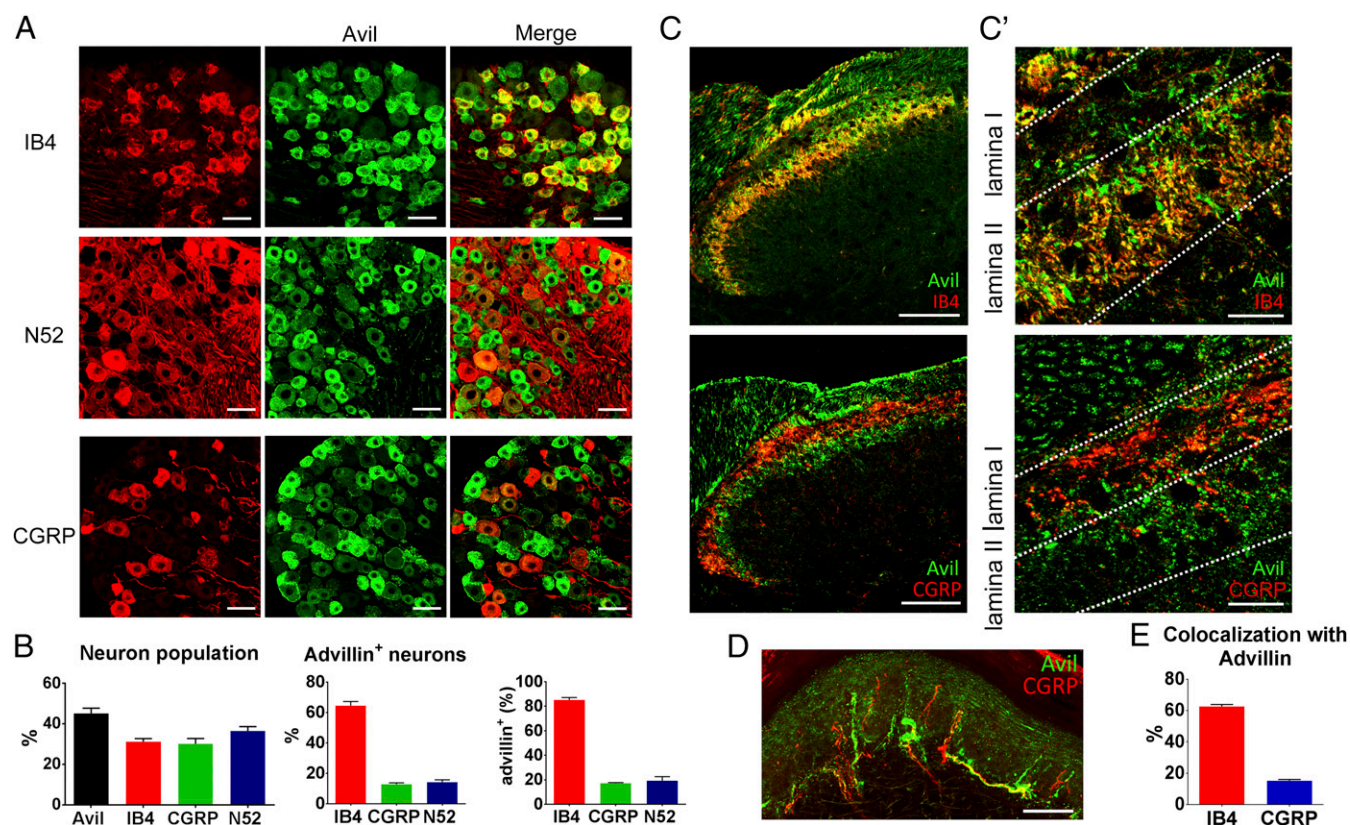


Fig. 1. Expression of advillin protein in adult DRG neurons and their central and peripheral projections. (A) Representative immunostaining of WT DRG sections show differential expression of advillin in different subsets of neurons. Neurons with high expression of advillin were mainly small-sized, IB4⁺, as shown in the merged images (Right). Advillin immunoreactivity was seldom found in DRG neurons stained with N52 or CGRP. (Scale bars: 50 μ m.) (B) To define advillin⁺ neurons, immunoreactive signals were clustered into two groups by K-means clustering (high as positive or low as negative). (Left) The ratios of advillin⁺, IB4⁺, CGRP⁺, and N52⁺ neurons in total DRG neuron population. (Center) Of advillin-expressing neurons, 64.53 \pm 2.73% were IB4⁺. (Right) Advillin was expressed in 85.15 \pm 1.96% IB4⁺ neurons. (C) In WT spinal-cord sections, advillin was distributed through the superficial dorsal laminae, predominantly in lamina I and II. In lamina I, advillin partially colocalized with CGRP. In lamina II, advillin is largely overlapped with IB4. (Scale bars: 100 μ m.) (C') High-magnification images highlight the advillin immunoreactivity in lamina I and II, which show dominant expression of CGRP and IB4, respectively. (Scale bars: 20 μ m.) (D) In WT skin, advillin immunoreactivity did not overlap with CGRP in afferent terminals projecting to epidermis. (Scale bar: 50 μ m.) (E) To characterize the advillin-marked layers in the spinal cord, the colocalization of advillin immunoreactivity with IB4 or CGRP was quantified. Advillin immunoreactivity colocalization with IB4 was 62.6 \pm 1.2% (n = 61) in lamina II and with CGRP 15.2 \pm 0.9% (n = 51) in lamina I.

Live imaging revealed that pathfinding of axon outgrowth was greatly affected by advillin KO (Fig. 3). The axon outgrowth of *Avil*^{+/-} DRG neurons was dynamic and accompanied by dynamic growth cones, as shown by time-lapse stacking images (Fig. 3A), whereas the axon outgrowth of *Avil*^{-/-} DRG neurons was often in a single direction and followed by few dynamic growth cones (Fig. 3B). On kymography, the coefficients of variation were higher for newly forming axons of *Avil*^{+/-} than *Avil*^{-/-} DRG neurons (Fig. 3C). Moreover, the velocities of axon extension and retraction were faster in *Avil*^{+/-} than *Avil*^{-/-} DRG neurons (Fig. 3D). Advillin KO specifically affected axon regeneration in IB4⁺ but not CGRP⁺ neurons. Advillin KO postponed or halted the neurite outgrowth of IB4⁺ neurons but had no effect on CGRP⁺ neurons (Fig. 3E).

Advillin Interacts with Focal-Adhesion-Related Proteins in Growth Cones.

Lines of evidence show that focal adhesion signaling modulates growth cones and consequently regulates axon regeneration of peripheral neurons (28). Thus, we examined whether advillin could affect the stabilization of filopodial tip adhesion in growth cones, where focal-adhesion complexes consist of scaffolding proteins, such as vinculin, to link with cytoskeletal components and signaling molecules, such as focal-adhesion kinase (FAK), required for successful axon regeneration (29–31). In growth cones of cultured DRG neurons, advillin immunoreactivity highly colocalized with

activated FAK (pFAK^{Y397}) and vinculin (SI Appendix, Fig. S6A). With advillin KO, FAK activation shifted from the vinculin-rich filopodial tips to vinculin-negative lamellipodia in growth cones (SI Appendix, Fig. S6B). The ratio of pFAK^{Y397} in lamellipodia to the central domain of the growth cone was significantly reduced in *Avil*^{-/-} (n = 74) compared with *Avil*^{+/+} (n = 42). In addition, advillin highly colocalized with myosin IIa in filopodial tips and lamellipodia of growth cones (SI Appendix, Fig. S6C). Advillin KO altered the myosin IIa protein clustering in growth cones from a spotty (and edge) distribution to a concentrated and edgeless distribution. The accumulation of myosin IIa in the lamellipodia was significantly lower in *Avil*^{-/-} (n = 58) than *Avil*^{+/+} (n = 67). Reduced edge clustering of vinculin, pFAK, and myosin IIa in growth cones with advillin KO might account for the loss of dynamic activity of axonal neurite outgrowth observed in the time-lapse live images in Fig. 3.

Advillin-Associated Protein Complex in Neuropathy. The above studies highlighted that advillin protein is highly associated with nascent focal-adhesion proteins, such as vinculin and FAK, in the very tips of filopodia and lamellipodia. We often observed isolated spots of advillin immunoreactivity surrounding neurite tips or aligned with traces of disappearing (or degrading) neurites (Fig. 4A and A'). Furthermore, myosin IIa always coexisted in the isolated spots of advillin immunoreactivity (Fig. 4B), similar to the coclustering of

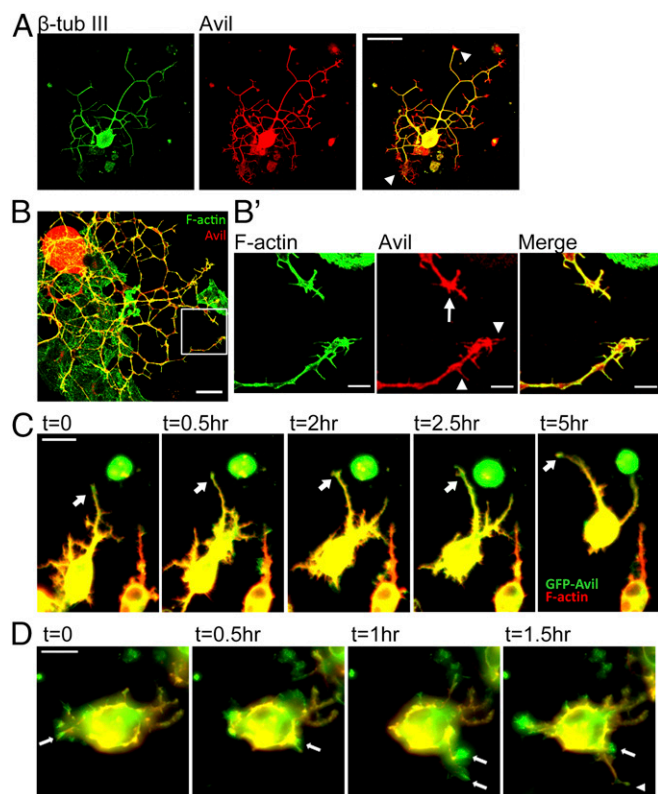


Fig. 2. Advillin expression in filopodia tips at active growth cones of regenerative DRG neurons and differentiating N2a cells. (A) In primary cultures of adult DRG neurons, advillin was distributed in soma and neurite shafts as well as axon terminals (growth cones) showing no expression of β -tubulin III. Arrowheads indicate two sites of growth cones. Green, β -tubulin III; red, advillin. (Scale bar: 50 μm .) (B) Advillin was highly colocalized with F-actin, especially in axon terminals of regenerating DRG neurons. Phalloidin staining, which marks F-actin, is in green and advillin staining is in red. (Scale bar: 20 μm .) (B') The inset of B shows a growth cone with advillin colocalized with F-actin in filopodia (arrowheads) and lamellipodia (arrow). (Scale bars: 5 μm .) (C and D) Live-imaging recording of differentiating DRG neurons cotransfected with GFP-advillin and LifeAct-tagRFP, which labels F-actin. (C) In live images, GFP-advillin always appeared at the very tips of growing neurites of differentiating N2a cells before F-actin. The arrow indicates the dynamic interaction between GFP-advillin and F-actin in the tip of a growing neurite. (Scale bar: 20 μm .) (D) During filopodia formation and maturation, advillin appeared at the tips of newly forming filopodia (spike-like structure marked by arrows), then F-actin followed behind with filopodia elongation (marked by an arrowhead). (Scale bar: 20 μm .)

advillin and myosin IIa in the filopodia tips or lamellipodia of growth cones (SI Appendix, Fig. S6C).

We wondered whether these isolated advillin-immunoreactivity spots were the remaining nascent focal adhesions after neurite retraction or artifacts of immunostaining. We thus used live-imaging to monitor the dynamics of growth cones in adult DRG neurons transfected with the advillin-GFP construct and found that advillin-containing neurite tips were often disconnected from retracting neurites (Fig. 4C). Time-lapse imaging showed advillin-containing neurite tips clearly shed during neurite retraction (Movie S4). The live-imaging data suggest that the shed neurite tips are nascent focal adhesions containing an advillin-associated protein complex.

We next tested whether this advillin-associated protein complex could be found in axonal regeneration of primary sensory neurons in vivo in the context of neuropathy. We hypothesized that in the context of peripheral neuropathy, advillin would be detectable in cerebrospinal fluid (CSF) if advillin-associated nascent focal adhesions are shed during active neurite retraction accompanied by

axonal regeneration. We analyzed the CSF of naive mice and EAE mice, a mouse model of multiple sclerosis that shows severe peripheral neuropathy associated with IB4⁺ sensory neurons (23). Advillin and myosin IIa protein was detectable in the CSF of EAE mice in the recovery phase, defined as after day 30 in the EAE model, with score 3 or higher, but was not detectable in naive healthy mice (Fig. 4D and E).

Thus, the advillin-associated protein complex might be a useful biomarker for diagnosis of peripheral neuropathy.

A Role for Advillin in EAE-Induced Neuropathic Pain. The above data suggest that advillin is involved in neurite outgrowth during axonal regeneration in vitro (cultured DRG neurons) and in vivo (recovery phase of EAE). Therefore, we tested the possible role of advillin in EAE-induced clinical symptoms and neuropathic pain. Clinical scores were higher for *Advillin*^{-/-} than WT mice from day 33 after EAE induction (Fig. 5A), while rotarod performance was similar (Fig. 5B). The result suggests that advillin could facilitate the recovery of the nervous system after inflammatory demyelinating damage.

We evaluated the neuropathic pain in the recovery phase. Consistent with clinical score evaluation, mechanical hyperalgesia (Fig. 5C), mechanical allodynia (SI Appendix, Fig. S7), and cold allodynia (Fig. 5D and E), observations were more severe for *Advillin*^{-/-} than WT mice. *Advillin*^{-/-} mice were hypersensitive to non-nociceptive cold stimulus at 15 °C, including shortening the latency to the first nocifensive behavior and increased nocifensive events (Fig. 5D and E). The aggravated EAE-induced nociceptive behaviors of *Advillin*^{-/-} mice again suggest that advillin could facilitate the recovery of neuropathy and neuropathic pain after EAE induction. The role of advillin was further validated by advillin knockdown in left side of lumbar DRGs, by which the EAE-induced mechanical allodynia was aggravated on the ipsilateral side compared with contralateral side (SI Appendix, Fig. S7).

Advillin Affects Neural Plasticity of IB4⁺ Central Afferents in the EAE Mouse Model. To dissect the possible mechanism of advillin KO aggravating the EAE-induced neuropathic pain, we analyzed neural plastic changes of spinal-cord dorsal horns in the recovery phase of EAE. In the EAE model, vinculin expression was abundant in the superficial dorsal horn of *Advillin*^{-/-} but not WT or naive mice of both genotypes (Fig. 6A). Increased vinculin expression principally appeared in lamina I of the spinal-cord dorsal horn (Fig. 6B) and largely colocalized with IB4 in the dorsal root and dorsal entry zone, with less colocalization with CGRP⁺ neurites in lamina I (Fig. 6C). In the EAE model, from normalized intensity means of lamina I; vinculin expression was significantly higher in *Advillin*^{-/-} than WT and naive mice (Fig. 6D). This phenomenon may reflect the disturbed interaction between vinculin and pFAK in regenerated afferents with advillin KO shown in cultured DRG neurons (SI Appendix, Fig. S6B). Additionally, in *Advillin*^{-/-} mice, IB4-marked dorsal-horn layers (mainly in lamina II in naive WT) were altered and overlapped with CGRP-marked layers (mainly in lamina I in naive WT mice) (Fig. 6E and E' and SI Appendix, Fig. S8). Of note, IB4⁺ dorsal-horn layers were partially disrupted in the mediolateral extent of lamina II in EAE *Advillin*^{-/-} mice (Fig. 6E'). The overlapping of CGRP- and IB4-labeled regions was significantly increased in EAE *Advillin*^{-/-} mice compared with other groups (Fig. 6F). Hence, advillin KO resulted in abnormal EAE-induced neural plasticity mainly in IB4⁺ central projections, related to nociception.

Advillin Plays a Role in Chemotherapy-Induced Peripheral Neuropathy. Clinically, oxaliplatin induces acute and chronic peripheral neuropathy consisting of cold-induced dysesthesia, paraesthesia, or pain in the face, upper limbs, and perioral regions (32, 33). To further validate a role for advillin in peripheral neuropathy, we tested whether advillin KO had an impact on oxaliplatin-induced cold allodynia, a key feature of oxaliplatin-induced peripheral neuropathy targeting on IB4⁺ DRG neurons (3). Similar to the

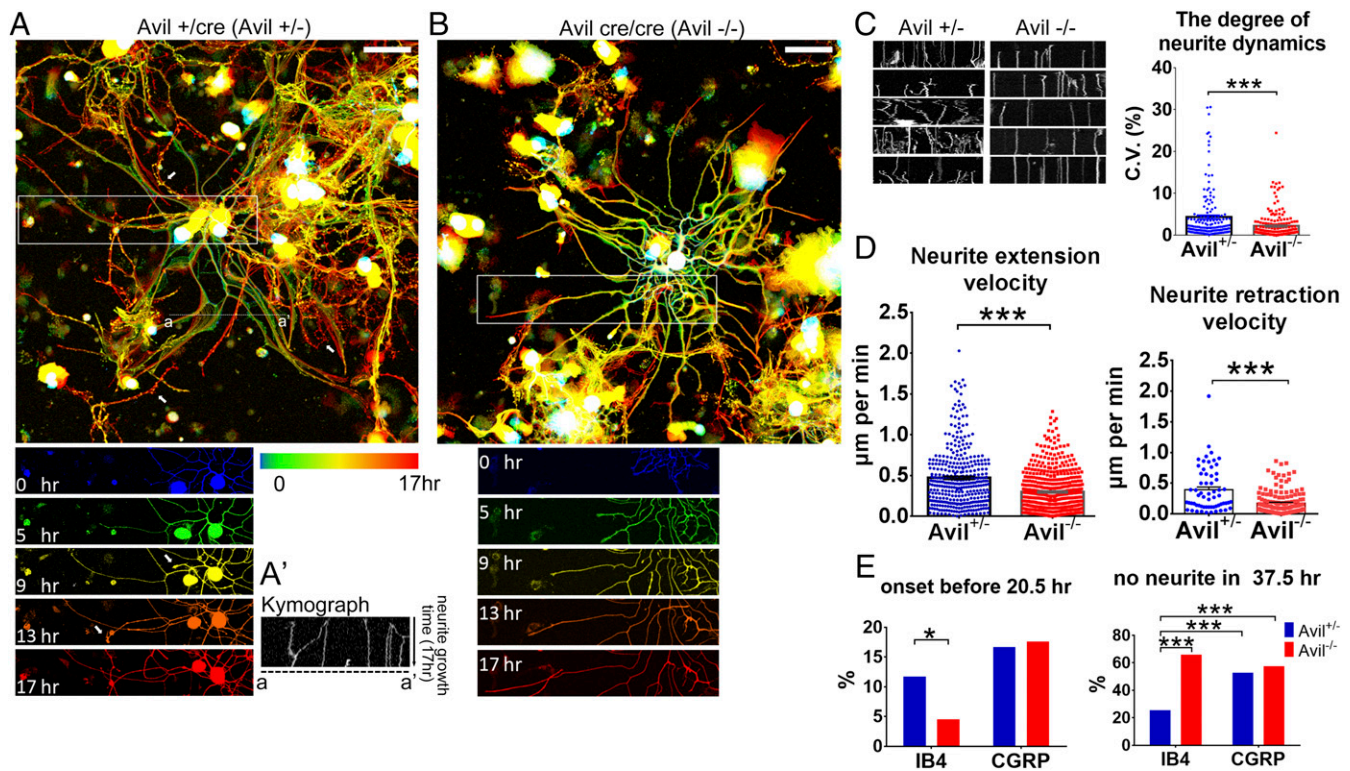


Fig. 3. Dynamics of axonal neurite outgrowth of DRG neurons on live imaging. (A and B) Representative kymographs of cultured DRG neurons of adult advillin-cre (*Avil^{+/cre}* or *Avil^{cre/cre}*):tdTomato mice (representing *Avil^{+/-}* or *Avil^{-/-}*, respectively). DRG were cultured and analyzed for axonal neurite outgrowth by live imaging. Time-lapse imaging recording started at 20.5 h after seeding. Cultured DRG neurons were imaged by confocal microscopy every 30 min for 17 h. (Upper) Thirty-four images of *Avil^{+/-}* or *Avil^{-/-}* DRG neurons were stacked with color projection indicating the spatial position of neurites over time. (Lower) The neurons of *Insets* (defined in *Upper* panels) at 0, 5, 9, 13, and 17 h are marked by colors. The white arrows indicate the tracts of growth cones, more dynamic in *Avil^{+/-}* than *Avil^{-/-}* DRG. (A') The dynamics of *Avil^{+/-}* neurites at the white dashed line within 17 h traced in a kymograph to show the position change of neurite shafts. (Scale bars: 100 μ m.) (C, Left) Representative kymographs of *Avil^{+/-}* and *Avil^{-/-}* neurites showing the tract dynamics of neurite position within 17 h. (Right) The change in the x axis value calculated as the coefficient of variation (c.v.) to show the tract dynamics. *Avil^{+/-}* $n = 164$, *Avil^{-/-}* $n = 191$. $***P < 0.001$. (D) Time-course images showing the velocity of neurite extension and retraction. Extension: *Avil^{+/-}* $n = 373$, *Avil^{-/-}* $n = 522$. Retraction: *Avil^{+/-}* $n = 62$, *Avil^{-/-}* $n = 162$. $***P < 0.001$. (E) Advillin KO selectively delayed axon regeneration in cultured IB4⁺ DRG neurons. After live recording, cultured cells were fixed and stained with CGRP antibody and IB4 to mark DRG neuron subtypes. *Avil^{+/-}*: IB4, $n = 94$; CGRP, $n = 72$. *Avil^{-/-}*: IB4, $n = 132$; CGRP, $n = 125$. $*P < 0.05$, $***P < 0.001$, χ^2 test (two-tailed).

EAE model, *Avil^{-/-}* mice had more severe cold allodynia than WT mice in the recovery phase of oxaliplatin treatment (Fig. 7A and B). Furthermore, unilaterally knocked down advillin in cervical DRGs aggravated cold allodynia in ipsilateral side compared with contralateral side (Fig. 7C and *SI Appendix*, Fig. S9). A single-dose treatment of oxaliplatin induced chronic cold allodynia in *Avil^{-/-}* mice, which suggests that advillin-mediated axon regeneration might be involved in resolving chemotherapy-induced neuropathic pain. If so, we may detect advillin in the CSF in mice treated with oxaliplatin, as shown in the EAE model (Fig. 4D). We thus collected CSF from naïve WT mice and those treated with oxaliplatin. Interestingly, both advillin and myosin IIa proteins were detected in mice showing short latency (<65 s) to cold stimulation at 2 or 4 d postoxaliplatin treatment (Fig. 7D). In contrast, advillin signal was not detectable (or in low level) in mice with long latency to cold stimulation. Advillin signal was mostly detected in the early phase (≤ 7 d) but seldom in the late phase (≥ 8 d) after oxaliplatin treatment (Fig. 7E).

Advillin Plays a Role in Peripheral Neuropathy Induced by CCI of the Sciatic Nerve. To better understand whether the advillin-mediated axonal regeneration is a critical factor contributing to the more severe neuropathic pain in *Avil^{-/-}* than WT mice, we further tested the effect of advillin KO on a local neuropathy model induced by CCI, followed by a decompression procedure. CCI treatment causes local neuropathy, which can be characterized by long-lasting neuropathic

pain lasting for more than 8 wk and neural degeneration in peptidergic afferents in skin, as well as a transient decrease (in 1 wk) of the IB4⁺ immunoreactivity in the spinal-cord dorsal horn (25, 26, 34). After sciatic compression, both *Avil^{+/-}* and *Avil^{-/-}* mice showed mechanical allodynia on the surgical side but not contralateral side (Fig. 8A and B). At postoperative day 14, a surgical decompression procedure was used to remove all ligatures on the sciatic nerve. After decompression, the mechanical allodynia was significantly reduced in *Avil^{+/-}* but not *Avil^{-/-}* mice. In the spinal cord, sciatic nerve compression significantly increased the expression of advillin in the ipsilateral dorsal horn at day 9, which then returned to the basal level of naïve mice at 2 wk after decompression (Fig. 8C). At day 9, the overlapping CGRP- and IB4-labeled regions were significantly increased on the ipsilateral side (\sim twofold) versus the contralateral side in both genotypes (Fig. 8D and E). Decompression reduced the CGRP-IB4 overlapping in the dorsal horn in *Avil^{+/-}* but not *Avil^{-/-}* mice (Fig. 8E). Moreover, advillin protein was detectable in the CSF from 9 of 23 CCI mice but not in CCI-decompression mice (Fig. 8F and G and *SI Appendix*, Fig. S10). Hence, the local nerve injury CCI model reveals a similar role for advillin in peripheral neuropathy, as shown in EAE and oxaliplatin models.

Discussion

Advillin is an actin-binding protein predominantly expressed in almost all somatosensory neurons in prenatal and early postnatal stages (17, 18). Here we successfully used advillin-specific antibodies

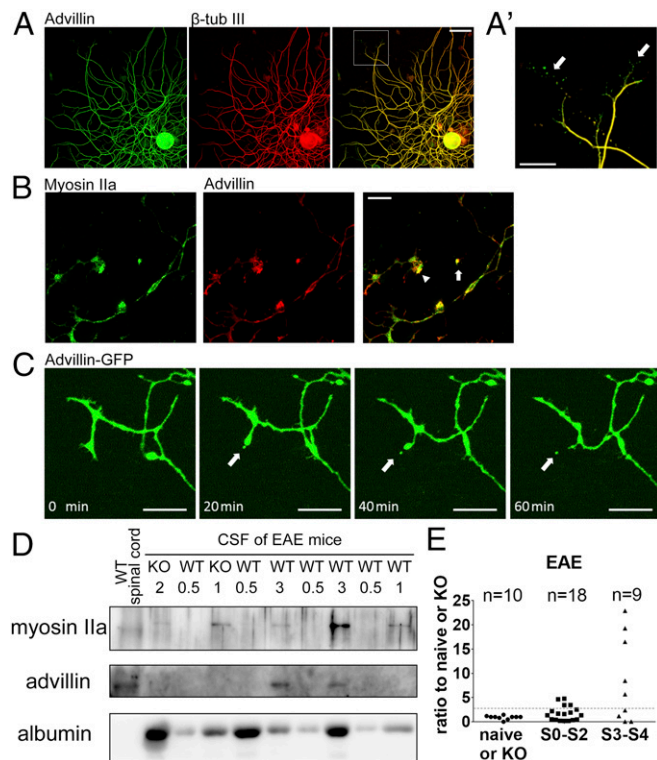


Fig. 4. Shedding the advillin-associated protein complex from neurite retraction. (A) Around neurite terminals of a cultured DRG neuron, spots of advillin immunoreactivity were observed (Inset A', arrows). (Scale bars: 50 μ m in A; 20 μ m in A'). (B) Myosin IIa colocalized with advillin in growth cones (arrowhead) of DRG neurons and in surrounding advillin-containing spots (arrow). (Scale bar: 10 μ m.) (C) In live imaging of DRG neurons transfected with advillin-GFP, advillin-GFP-containing neurite tips (arrow) were shed with neurite retraction (as seen in Movie S4). (Scale bars: 20 μ m.) (D) Representative Western blot analysis of advillin and myosin IIa protein levels in the CSF of EAE mice. CSF samples were collected from EAE mice in the recovery phase. Each lane was loaded with a 4- μ L CSF sample or 6- μ g WT spinal cord lysates as a positive control. Albumin was a loading control. The number below the genotype indicates the EAE clinical score on the day of CSF collection. (E) Quantification of advillin expression in CSF samples. The dotted line is the threshold level (mean of naive and KO samples + 5 \times SD) to define positive advillin expression.

to demonstrate its expression profile shifting to IB4⁺ DRG neurons in adulthood and the involvement of the advillin protein complex in the dynamic formation of growth cones during axonal regeneration. This cell-type-specific expression highlights the selective effect of advillin KO on the regenerative capability of cultured IB4⁺ but not CGRP⁺ DRG neurons. Accordingly, in the context of EAE-induced neuropathy, *Avil*^{-/-} mice showed abnormal neural plasticity of central projections of IB4⁺ DRG neurons, associated with more severe EAE symptoms and stronger neuropathic pain compared with WT littermates. Furthermore, *Avil*^{-/-} mice developed more severe chronic cold allodynia than did WT mice in oxaliplatin-induced peripheral neuropathy. With local nerve injury induced by CCI, *Avil*^{-/-} mice were blunted to surgical decompression, which effectively corrected the abnormal neuroplasticity of IB4⁺ central projections and attenuated the mechanical allodynia in WT mice. Our study suggests that advillin plays an important role in promoting axon regeneration of IB4⁺ sensory neurons and thus facilitates recovery from peripheral neuropathy and neuropathic pain.

IB4⁺ DRG neurons belong to the nonpeptidergic nociceptors that are largely involved in pain associated with peripheral neuropathy induced by chemotherapy, chronic constriction, and EAE (23, 35, 36). For example, nerve injury-induced mechanical allodynia is significantly reduced when IB4-binding afferent neurons

are specifically deleted by the toxin saporin (37). Previous studies have shown that glial cell-derived neurotrophic factor, a trophic factor of IB4⁺ DRG neurons, produces effective analgesia by reversing nerve injury-induced plasticity and sensory abnormalities that develop in neuropathic pain models (38).

Peripheral nerves are capable of regeneration after nerve injury (39). In the context of peripheral neuropathy, axon regeneration of nociceptors to sensory targets is essential for resolving neuropathic pain. The capacity for axon regeneration varies among different subsets of nociceptors. For example, decompression in rats with CCI causes peripheral axon regeneration of substance P⁺ but not CGRP⁺ nerves and thus relieves neuropathic pain (25). In contrast, the capacity of DRG neurons for central regeneration is limited. CGRP⁺ but not IB4⁺ sensory nerves are able to sprout into adjacent spinal segments denervated by dorsal rhizotomy (11). However, the capacity for axon regeneration of IB4⁺ DRG neurons is largely unknown.

During axon regeneration, multiple processes are required to generate a growth cone, including stimulus reception, calcium signaling, cytoskeletal reorganization, and material transportation (40). The subcellular localization of advillin in the very tips of regenerating DRG neurons highlights its important role in growth cone formation. On live imaging, the growth cones of regenerative axons were less dynamic in *Avil*^{-/-} than *Avil*^{+/-} DRG neurons. Thus, advillin may have a role in modulating cytoskeletal reorganization during growth cone formation. Although the exact enzymatic role of advillin is unclear, advillin may act like villin by bundling and severing F-actin in response to intracellular calcium signaling (21).

FAK signaling controls neurite outgrowth and branching (41–43). Autophosphorylation at Y397 of FAK, when recruited to adhesion sites, is triggered and required for full activation of FAK (44). In growth cones of DRG neurons, advillin clustered with Y397-phosphorylated FAK and vinculin, a scaffold protein for

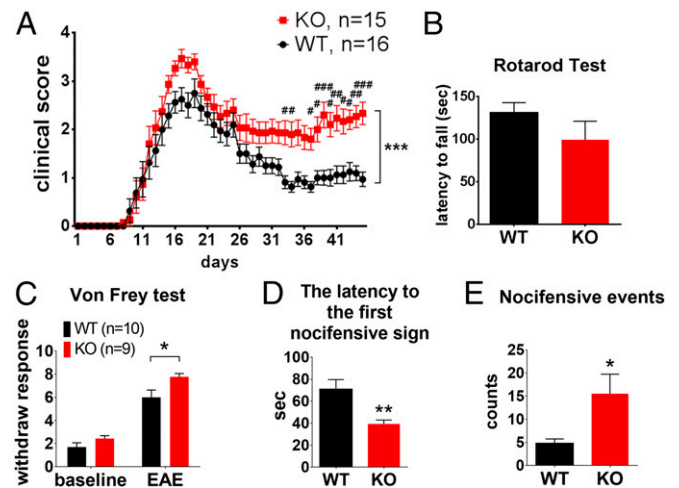


Fig. 5. Effect of advillin KO on EAE-induced symptoms and neuropathic pain. (A) EAE was induced in *Avil*^{-/-} (KO) and WT littermates, and disease severity was monitored by daily clinical scoring for 45 d. Data were analyzed by two-way ANOVA [interaction $F_{(44, 1,305)} = 2.103$, $P < 0.0001$; time $F_{(44, 1,305)} = 36.1$, $P < 0.0001$; genetic effect $F_{(1, 1,305)} = 159.3$, $P < 0.0001$], followed by post hoc tests of Sidak's multiple-comparison test. *** $P < 0.001$ vs. WT; # $P < 0.05$, ### $P < 0.01$, ### $P < 0.001$ for genotype difference at specific times. (B) Coordination of WT and KO mice in the recovery phase during the rotarod test. WT, $n = 8$, KO, $n = 6$. (C) Mechanical hyperalgesia measured by von Frey test before EAE induction (baseline) and in recovery phases of EAE. Data were analyzed by two-way ANOVA [interaction $F_{(1, 18)} = 4.872$, $P = 0.04$; treatment $F_{(1, 18)} = 324.9$, $P < 0.0001$; genotype effect $F_{(1, 18)} = 7.156$, $P = 0.015$], followed by Sidak's multiple-comparison test (* $P < 0.05$). (D and E) Cold allodynia measured by the cold plate at 15 $^{\circ}$ C. The recording duration was 150 s WT, $n = 15$, KO, $n = 13$. (* $P < 0.05$, ** $P < 0.01$ vs. WT.)

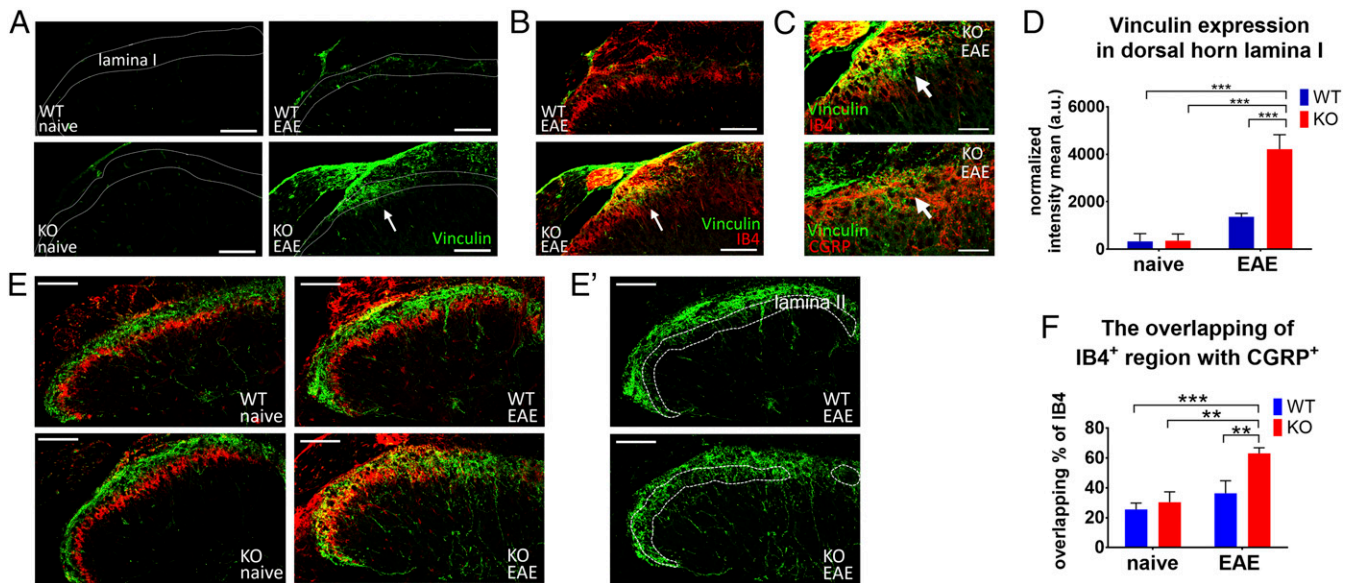


Fig. 6. Advillin KO resulted in abnormal neural plasticity in the spinal dorsal horn in the recovery phase of EAE models. (A) Vinculin expression in superficial dorsal horns (arrow) of naive and EAE mice in both genotypes. (Scale bars: 100 μ m.) (B) EAE-induced increased vinculin expression mainly found in dorsal lamina I (arrow) but not lamina II of KO mice, as marked by IB4 expression. (Scale bars: 100 μ m.) (C) In magnified images of lamina I, vinculin expression was found partly in IB4⁺ afferents but scarcely colocalized with CGRP⁺ afferents. (Scale bars: 50 μ m.) (D) Quantitative analysis of vinculin expression in the spinal-cord dorsal horn. The mean intensity of vinculin immunoreactivity in dorsal lamina I was quantified and normalized with background. WT-naive: $n = 2, n = 3$; KO-naive: $n = 2, n = 3$; WT-EAE: $n = 3, n = 10$, KO-EAE: $n = 3, n = 9$. Data were analyzed by two-way ANOVA [interaction $F_{(1, 21)} = 6.348, P = 0.0199$; treatment $F_{(1, 21)} = 19.06, P = 0.0003$; genetic effect $F_{(1, 21)} = 6.587, P = 0.018$], followed by Tukey's multiple-comparison test ($***P < 0.001$). (E) In the recovery phase of EAE, advillin KO disrupted the trajectory of CGRP⁺ and IB4⁺ central projections, which were clearly segregated in lamina I and II, respectively, in WT-EAE, WT-naive, and KO-naive mice. (Scale bars: 100 μ m.) (E') IB4⁺ areas marked with dashed lines highlight overlap with the CGRP⁺ layer (in green) in the spinal-cord dorsal horn of KO-EAE but not WT-EAE mice. (Scale bars: 100 μ m.) (F) Quantification of overlap of IB4- and CGRP-covered areas calculated as a percentage of the IB4⁺ region. L4 and L5 of spinal cords from naive or EAE mice in the recovery phase were collected for analysis. WT-naive: $n = 3, n = 6$; KO-naive: $n = 2, n = 7$; WT-EAE: $n = 3, n = 9$, KO-EAE: $n = 4, n = 18$. Data were analyzed by two-way ANOVA [interaction $F_{(1, 36)} = 3.032, P = 0.0902$; treatment $F_{(1, 36)} = 11.88, P = 0.0015$; genetic effect $F_{(1, 36)} = 6.32, P = 0.0166$], followed by Tukey's multiple-comparison test ($***P < 0.005, **P < 0.01$).

FAK (45). Advillin seems to be required for the proper dynamic organization of the focal-adhesion machinery, because advillin KO resulted in dislocation of activated FAK clustering from filopodial tips to lamellipodia. Notably, signaling through FAK promotes integrin-dependent growth-cone motility and is required for proper neurite outgrowth and guidance in vitro and in vivo (31). In agreement with this FAK function, our *Avil*^{-/-} DRG neurons showed reduced velocity of neurite extension and retraction during axon regeneration. In addition, the interaction between advillin and myosin IIa may account for the proper growth-cone activity of DRG neurons. Emerging data have shown that myosin II is required for fast sensory axon outgrowth on laminin (46); activation of myosin IIa contributes to the dynamics of filopodia and lamellipodia of growth cones (47–49). Moreover, myosin IIa and vinculin show cooperation in axonal outgrowth rates and the organization of growth-cone cytoskeletal components (50). Vinculin can influence filopodia motility in neuronal growth cones (51) and contributes to neurite outgrowth via redistribution and adhesion–cytoskeletal coupling (50, 52). Taking these data together, we find that advillin may be involved in FAK signaling and myosin II/vinculin-dependent adhesion complexes to modulate actin dynamics in growth cones.

A role for advillin in growth-cone formation and dynamics could have potential clinical application. Unexpectedly, we found that after neurite retraction, the advillin-associated nascent focal-adhesion protein complex often remained in the culture substrate after being “shed.” This in vitro phenomenon was recaptured in vivo by detecting advillin protein in the CSF of EAE mice with high (worse) clinical scores in the recovery phase, mice with oxaliplatin-induced cold allodynia, and mice with compression injury of the sciatic nerve. Because advillin is a sensory neuron-specific protein, the detection of advillin in the CSF could be a

bio-signature for diagnosis of peripheral neuropathy associated with IB4⁺ nociceptors. Further investigation is needed to optimize the detection ranges and sensitivity of advillin in CSF, because current evidence is not yet comprehensive and nerve-injury conditions might vary among models and among mice.

Neuropathic pain is defined as “pain initiated or caused by a primary lesion or dysfunction in the nervous system” (2). Proper axon regeneration would influence neuropathic pain (4). In the EAE mouse model, neuropathic pain could develop and be maintained even if clinical symptoms have largely resolved (23). As a peripheral neuropathy model, oxaliplatin induces sensory axon degeneration of intraepidermal nerve fiber (53, 54). Our study implicates that the aggravated EAE-induced and oxaliplatin-induced neuropathic pain symptoms in *Avil*^{-/-} mice may be caused by impaired axon regeneration, especially in IB4⁺ nociceptors. Thus, trophic factors promoting IB4⁺ axon regeneration may provide effective analgesia for multiple sclerosis patients.

In the work by Hasegawa et al. (18), advillin was required for the remodeling of central trigeminal axon innervations with whisker lesions induced in neonatal mice. Advillin may have a role in neural plasticity after nerve injury. In *Avil*^{-/-} EAE mice, vinculin showed high expression in superficial dorsal horns, especially in lamina I. Because advillin is involved in regulating the FAK/vinculin complex in growth cones, lack of advillin may disturb focal-adhesion complex formation and axon regeneration and thus alter the distribution of vinculin in growth cones. Furthermore, the distinct boundary between CGRP⁺ and IB4⁺ afferents in the spinal-cord dorsal horn (as shown in WT and naive *Avil*^{-/-} mice) was disturbed in *Avil*^{-/-} EAE mice: IB4⁺ afferents shifted toward lamina I and distributed unevenly in both layers I and II, whereas CGRP⁺ afferents expanded and occupied the discontinued region

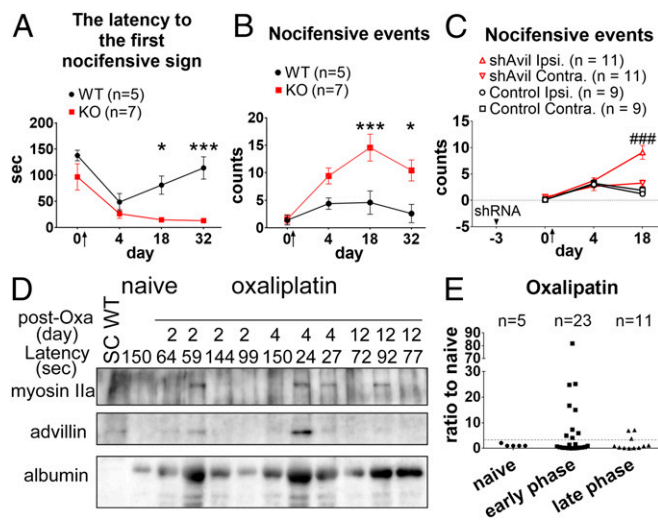


Fig. 7. Effect of advillin KO and knockdown on oxaliplatin-induced peripheral neuropathy. (A and B) Cold allodynia was induced by oxaliplatin treatment (15 mg/kg, i.p.) and measured by the cold plate at 15 °C. The baseline responses were recorded before oxaliplatin treatment (day 0), and the time of treatment is marked by arrows. Data were analyzed by two-way ANOVA, followed by Sidak's multiple-comparison test. For latency of first nocifensive sign, interaction $F_{(3, 30)} = 2.964$, $P = 0.0478$; time $F_{(3, 30)} = 12.89$, $P < 0.0001$; genetic effect $F_{(1, 10)} = 19.88$, $P = 0.0012$. For nocifensive events, interaction $F_{(3, 30)} = 2.978$, $P = 0.0471$; time $F_{(3, 30)} = 7.592$, $P = 0.0006$; genetic effect $F_{(1, 10)} = 22.3$, $P = 0.0008$. * $P < 0.05$, *** $P < 0.001$ vs. WT. (C) Effect of unilateral knockdown of DRG advillin on oxaliplatin-induced cold allodynia. CG/Avil-shRNA polyplexes or control vehicle was injected to the left side of forepaws 3 d before oxaliplatin. Nocifensive events of left and right forepaws were separately counted. Data were analyzed by two-way ANOVA, followed by Sidak's multiple-comparison test [interaction $F_{(6, 72)} = 11.65$, $P < 0.0001$; genetic effect $F_{(3, 36)} = 10.79$, $P < 0.0001$]. ### $P < 0.001$ vs. contralateral side. The arrow marks the time of oxaliplatin injection. (D) A representative Western blot for detection of advillin and myosin IIa protein in the CSF of oxaliplatin-treated mice. Each lane was loaded with a 5- μ L CSF sample or 6- μ L WT spinal cord lysates as a positive control. (E) Quantification of advillin expression in CSF samples. The dotted line is the threshold level (mean of naïve samples + 5 \times SD) to define the positive advillin expression.

of IB4⁺ layers. The reduced velocity of IB4⁺ neurite outgrowth may account for the "partial retraction" of IB4⁺ afferents from layer II to layer I in *Avil*^{-/-} EAE mice. Similarly, spinal cord injury-induced neuropathic pain is correlated with disturbed and expanded sprouting of IB4⁺ afferents in the spinal-cord dorsal horn (55). Although we do not know the pathological meaning of the mingling of CGRP⁺ and IB4⁺ afferents in superficial layers of the spinal cord, the data suggest that advillin might be required for setting a proper axon regeneration program after nerve injury. Similarly, in the CCI-decompression model, advillin is required for the decompression therapy to correct the CCI-induced abnormal mingling of CGRP⁺ and IB4⁺ afferents in the dorsal horn and to relieve neuropathic pain.

Although we have demonstrated a role for advillin in growth cones and axonal regeneration of IB4⁺ DRG neurons in adulthood, the precise role of advillin in neural development, neural plasticity, and neuropathy is still a conundrum. Advillin expression in DRG is rich in the early developmental stages (17, 18). Obviously, advillin has a role in axon regeneration and accompanying neural plasticity. However, advillin KO did not affect neural development of the somatosensory system. Why organisms invest so much energy in producing advillin transcripts for no function is unclear. Advillin may exist to be available for any emergency and to secure normal neural regeneration (and development) in case of nerve injury. Unfortunately, this role of advillin might be not seen in mice housed in a well-controlled specific pathogen-free environment. Further studies are needed

to determine whether *Avil*^{-/-} mice would have abnormal neural development in a stressful housing environment.

In conclusion, advillin highlighting the axis of growth cone–axon regeneration–neural plasticity is critical for harmonious recovery from neural injury. Moreover, clinically, advillin could be a bio-signature for diagnosis of peripheral neuropathy. Nevertheless, although we found no compensation of villin protein expression in DRG, we cannot exclude the possible gene redundancy of other villin/gelsolin family members contributing to the pain phenotypes in *Avil*^{-/-} mice in a context of peripheral neuropathy.

Materials and Methods

Animals. All procedures followed the *Guide for the Care and Use of Laboratory Animals* (56) and were approved by the Institutional Animal Care and Use Committee of Academia Sinica. The *Avil*^{Cre} mouse line (19) was a kind gift from Fan Wang, Duke University Medical Center, Durham, NC, and was crossed with CAG-Td-tomato or CAG-GFP Cre reporter mice. *Avil*^{Cre/Cre} mice were used as advillin-KO mice, because advillin exon2 is replaced by a Cre-cassette and homozygous knockin mice do not express any advillin mRNA (18, 19). For behavioral studies, *Avil*^{Cre} mice were backcrossed to C57BL/6J mice for 10 generations to establish a congenic strain. WT mice (*Avil*^{+/+}) and advillin-KO mice (*Avil*^{Cre/Cre} or *Avil*^{-/-}) used in behavioral studies were offspring from heterozygotes (*Avil*^{+/-}) intercrossed. For Western analysis of CSF samples, C57BL/6J and BALB/cByJNarl mice were used for EAE induction and oxaliplatin treatment, respectively. Lumbar parts of DRG and spinal cord were collected for biochemistry, cell culture, and immunostaining. Unless described, adult mice at 8- to 12-wk-old were used in all studies.

Antibody Preparation, Mass Spectrometry, and Co-IP. A peptide "DGEYKYPVEVLKGGQNL" corresponding to the headpiece domain of mouse advillin was synthesized and conjugated with ovalbumin. The synthetic peptides were applied to boosting rabbits to generate the polyclonal antibody of advillin. Sera were collected and purified with columns coupled with corresponding antigen. Details of MS and Co-IP are described in *SI Appendix*.

Western Blot Analysis. Primary antibodies used in Western blot were rabbit polyclonal antiadvillin (1 μ g/mL), mouse monoclonal anti- β -actin (1:10,000; Sigma), mouse anti-N-cadherin (1:1,000; Millipore), mouse monoclonal anti-myosin IIa (1:500, ab55456; Abcam), and rabbit IgG isotype control (1 μ g/mL), and rabbit antialbumin (1:5,000, both GeneTex). Details are described in *SI Appendix*.

Cell Culture, Plasmid Construction, and Transfection. The mouse N2a neuroblastoma cell line was obtained from the American Type Culture Collection (#CCL-107). The primary culture of DRG neurons was as described previously (57). DRG neurons were transfected with plasmids by nucleofection as described previously (58), with some modification. Details of cell culture, plasmid construction, and transfection are given in *SI Appendix*.

Immunohistochemistry. Primary antibodies or fluorescence-conjugated agents used in the study were mouse antineurofilament 200 (N52, 1:1,000; Millipore), guinea pig antiserum P (1:2,000; Neuromics), goat anti-CGRP (1:1,000; Serotec), mouse monoclonal antimyosin IIa (1:500, ab55456; Abcam), Alexa Fluor 594 isolectin GS-IB4 (1:1,000; Invitrogen), mouse anti- β -tubulin III (1:3,000; Abcam), mouse anti- α -tubulin (1:5,000; Abcam), rabbit anti-pFAK^{Y397} (1:1,000; Invitrogen), mouse antivinuculin (1:1,000; Sigma), and Alexa Fluor 488 phalloidin (1:1,000; Invitrogen). For advillin antibody, titers of 1 μ g/mL were applied to the DRG and spinal cord tissue sections, and 5 μ g/mL of adsorbed advillin antibody was used for cutaneous tissue sections. Details of immunofluorescence and image quantification are described in *SI Appendix*.

Live Imaging. N2a cells were transfected with LifeAct-tagRFP (Ibidi) and GFP-advillin. For DRG, *Avil*^{Cre::GFP} or *Avil*^{Cre::tdTomato} or *Avil*^{Cre::tdTomato} 12-wk-old mice were used. Details of live imaging are given in *SI Appendix*.

Neuropathic Pain Models. EAE induction involved use of myelin oligodendrocyte glycoprotein (MOG; MDBio) peptide 35–55 emulsified with an equal volume of complete Freund's adjuvant (Sigma) in PBS, as previously described (23). Details of EAE induction and clinical scoring, the oxaliplatin model (59), and the CCI-decompression model (25) are given in *SI Appendix*.

Behavior Assays. Mechanical hypersensitivity (hyperalgesia or allodynia) was evaluated by the von Frey test with a 0.02-g filament (60) or with a simplified up–down method (61). Cold allodynia was assessed by the cold plate test

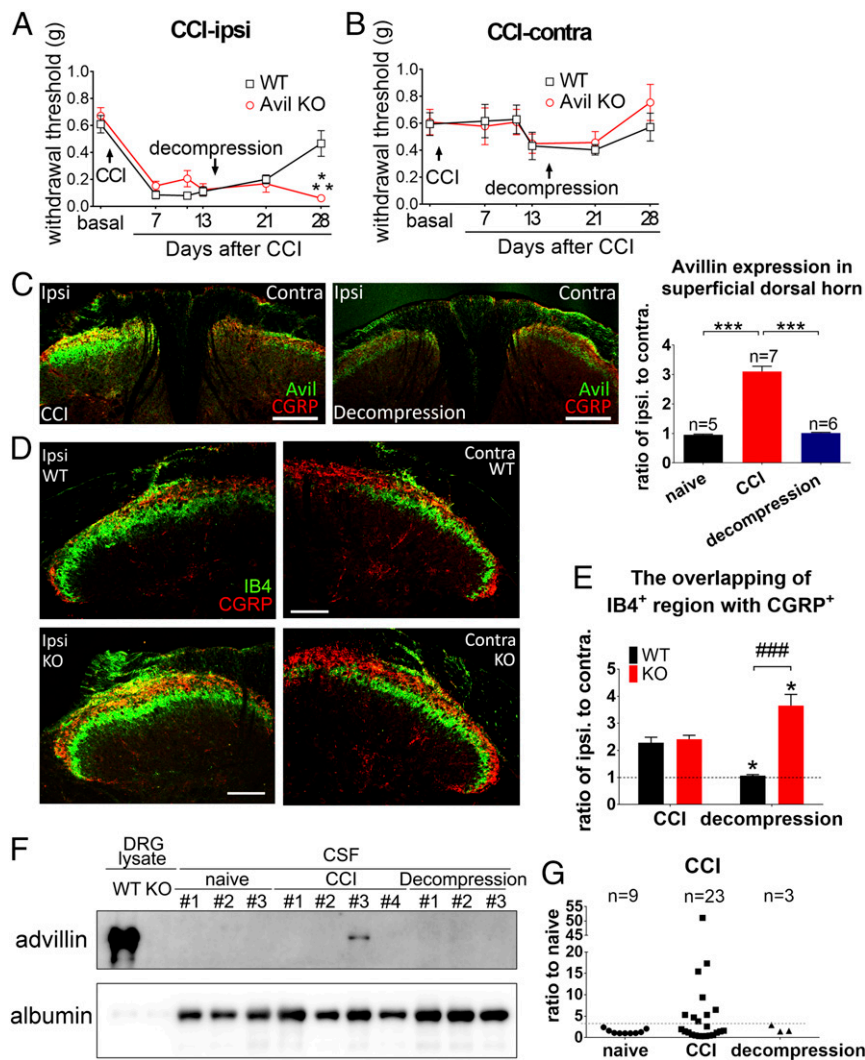


Fig. 8. Effect of advillin KO on neuropathic pain and neuroplasticity associated with local nerve injury from compression of the sciatic nerve. (A and B) Mechanical allodynia was induced by CCI of the left sciatic nerve and assessed by using the simplified up-down method. After CCI, the mechanical threshold was significantly decreased in the ipsilateral hindpaw of both WT and KO mice but not the contralateral paw. At 14 d after CCI, mice underwent surgical decompression to remove all ligatures on the sciatic nerve. At day 28 (14 d after decompression), the mechanical threshold was restored in WT but not KO mice. Data were analyzed by two-way ANOVA [ipsilateral side: time $F_{(5, 70)} = 28.21$, $P < 0.001$; genotype $F_{(1, 14)} = 1.087$, $P = 0.3148$; interaction $F_{(5, 70)} = 6.418$, $P < 0.001$], followed by Sidak's multiple-comparison test. *** $P < 0.001$ vs. WT. (C) Advillin immunoreactivity in the spinal cord dorsal horn was significantly increased in the ipsilateral side of CCI mice (at postoperative day 9) compared with naive and CCI-decompression mice. *** $P < 0.001$. (Scale bars: 200 μm.) (D) Representative images of CGRP and IB4 immunoreactivity in the spinal cord dorsal horn of CCI (day 9) mice showed increased CGRP-IB4 overlapping in the ipsilateral but not contralateral side in both WT and KO mice. (Scale bars: 100 μm.) (E) Quantitative analysis of IB4-CGRP overlapping area in the spinal-cord dorsal horn in CCI and CCI-decompression mice. CCI induced a twofold increase of IB4-CGRP overlapping in the ipsilateral vs. contralateral side, which was recovered after decompression in WT but not KO mice. Data were analyzed by two-way ANOVA, followed by Tukey's post hoc test [interaction $F_{(1, 25)} = 22.65$, $P < 0.0001$; treatment $F_{(1, 25)} = 0.002$, $P = 0.97$; genotype $F_{(1, 25)} = 27.71$, $P < 0.0001$]. * $P < 0.05$ vs. CCI; ### $P < 0.001$ between genotypes. (F) Western blot analysis of advillin protein level in CSF of CCI mice. CSF samples were collected from naive, CCI, and decompression mice. Each lane was loaded with a 6-μL CSF sample or 0.5 μg WT DRG lysates as a positive control. (G) Quantification of advillin expression in CSF samples. The dotted line is the threshold level (mean of naive samples + 5 × SD) to define the positive advillin expression.

with an innocuous temperature (59). The rotarod test was performed on a rotarod machine with automatic timers and falling sensors (MK-660D; Muromachi KiKai), as described previously (23). The experimenters for behavioral assays were blinded to the mouse genotypes. Additional information of behavioral assays is given in *SI Appendix*.

Advillin Knockdown. In the EAE model, shRNA plasmids were mixed with JetPEI (Polyplus-transfection SA) and injected to left sciatic nerves. In oxaliplatin model, shRNA plasmids were mixed with cationized gelatin, a kind gift from Yasuhiko Tabata at Kyoto University, Japan, and subcutaneously injected to the left forepaw. Details are described in *SI Appendix*.

CSF Collection. CSF was collected as described previously (62). Details are given in *SI Appendix*.

Statistical Analysis. Data in all figures are presented as mean ± SEM. The number of mice in a given study is indicated by "n." Statistical comparison involved use of GraphPad Prism6. Analyses involved ANOVA followed with the Sidak or Tukey analysis. The criterion for significant difference was set at $P < 0.05$.

ACKNOWLEDGMENTS. We thank Dr. Fan Wang for kindly providing the advillin-Cre mouse; Dr. Chao-Kuen Lai (Taiwan Mouse Clinic, Academia Sinica) for assistance in designing the cold allodynia assay; Dr. Yasuhiko Tabata for the generous gift of cationized gelatin; Ms. I-Ching Wang for help with experimental autoimmune encephalomyelitis induction; and the National RNAi Core Facility at Academia Sinica in Taiwan for providing shRNA reagents. This work was supported by the Institute of Biomedical Sciences, Academia Sinica, and by grants from the Ministry of Science and Technology, Taiwan (MOST105-2320-B-001-018-MY3, MOST107-2321-B-001-020, and MOST107-2319-B-001-002).

1. Costigan M, Scholz J, Woolf CJ (2009) Neuropathic pain: A maladaptive response of the nervous system to damage. *Annu Rev Neurosci* 32:1–32.
2. Merskey H, Bogduk N (1994) *Classification of Chronic Pain: Descriptions of Chronic Pain Syndromes and Definitions of Pain Terms* (IASP, Seattle), 2nd Ed.
3. Joseph EK, Chen X, Bogen O, Levine JD (2008) Oxaliplatin acts on IB4-positive nociceptors to induce an oxidative stress-dependent acute painful peripheral neuropathy. *J Pain* 9:463–472.
4. Zimmermann M (2001) Pathobiology of neuropathic pain. *Eur J Pharmacol* 429:23–37.
5. Dworkin RH, et al. (2003) Advances in neuropathic pain: Diagnosis, mechanisms, and treatment recommendations. *Arch Neurol* 60:1524–1534.
6. Løseth S, Stålberg E, Jorde R, Mellgren SI (2008) Early diabetic neuropathy: Thermal thresholds and intraepidermal nerve fibre density in patients with normal nerve conduction studies. *J Neurol* 255:1197–1202.
7. Cheng HT, et al. (2013) Increased axonal regeneration and swellings in intraepidermal nerve fibers characterize painful phenotypes of diabetic neuropathy. *J Pain* 14: 941–947.
8. Navarro X, Vivó M, Valero-Cabré A (2007) Neural plasticity after peripheral nerve injury and regeneration. *Prog Neurobiol* 82:163–201.
9. Landowski LM, Dyck PJ, Engelstad J, Taylor BV (2016) Axonopathy in peripheral neuropathies: Mechanisms and therapeutic approaches for regeneration. *J Chem Neuroanat* 76:19–27.
10. Basbaum AI, Bautista DM, Scherrer G, Julius D (2009) Cellular and molecular mechanisms of pain. *Cell* 139:267–284.
11. Belyantseva IA, Lewin GR (1999) Stability and plasticity of primary afferent projections following nerve regeneration and central degeneration. *Eur J Neurosci* 11: 457–468.
12. Gardiner NJ (2011) Integrins and the extracellular matrix: Key mediators of development and regeneration of the sensory nervous system. *Dev Neurobiol* 71: 1054–1072.
13. Tucker BA, Rahimtula M, Mearow KM (2006) Laminin and growth factor receptor activation stimulates differential growth responses in subpopulations of adult DRG neurons. *Eur J Neurosci* 24:676–690.
14. Harvey P, Gong B, Rossomando AJ, Frank E (2010) Topographically specific regeneration of sensory axons in the spinal cord. *Proc Natl Acad Sci USA* 107: 11585–11590.
15. Leclere PG, et al. (2007) Impaired axonal regeneration by isolectin B4-binding dorsal root ganglion neurons in vitro. *J Neurosci* 27:1190–1199.
16. Akopian AN, Wood JN (1995) Peripheral nervous system-specific genes identified by subtractive cDNA cloning. *J Biol Chem* 270:21264–21270.
17. Ravenall SJ, Gavazzi I, Wood JN, Akopian AN (2002) A peripheral nervous system actin-binding protein regulates neurite outgrowth. *Eur J Neurosci* 15:281–290.
18. Hasegawa H, Abbott S, Han BX, Qi Y, Wang F (2007) Analyzing somatosensory axon projections with the sensory neuron-specific Advillin gene. *J Neurosci* 27: 14404–14414.
19. Zhou X, et al. (2010) Deletion of PIK3C3/Vps34 in sensory neurons causes rapid neurodegeneration by disrupting the endosomal but not the autophagic pathway. *Proc Natl Acad Sci USA* 107:9424–9429.
20. Shibata M, et al. (2004) Type F scavenger receptor SREC-1 interacts with advillin, a member of the gelsolin/villin family, and induces neurite-like outgrowth. *J Biol Chem* 279:40084–40090.
21. Khurana S, George SP (2008) Regulation of cell structure and function by actin-binding proteins: Villin's perspective. *FEBS Lett* 582:2128–2139.
22. Thorburn KC, Paylor JW, Webber CA, Winship IR, Kerr BJ (2016) Facial hypersensitivity and trigeminal pathology in mice with experimental autoimmune encephalomyelitis. *Pain* 157:627–642.
23. Wang IC, Chung CY, Liao F, Chen CC, Lee CH (2017) Peripheral sensory neuron injury contributes to neuropathic pain in experimental autoimmune encephalomyelitis. *Sci Rep* 7:42304.
24. Starobova H, Vetter I (2017) Pathophysiology of chemotherapy-induced peripheral neuropathy. *Front Mol Neurosci* 10:174.
25. Tseng TJ, Chen CC, Hsieh YL, Hsieh ST (2007) Effects of decompression on neuropathic pain behaviors and skin reinnervation in chronic constriction injury. *Exp Neurol* 204: 574–582.
26. Bennett GJ, Xie Y-K (1988) A peripheral mononeuropathy in rat that produces disorders of pain sensation like those seen in man. *Pain* 33:87–107.
27. Marks PW, Arai M, Bandura JL, Kwiatkowski DJ (1998) Advillin (p92): A new member of the gelsolin/villin family of actin regulatory proteins. *J Cell Sci* 111:2129–2136.
28. Eva R, Fawcett J (2014) Integrin signalling and traffic during axon growth and regeneration. *Curr Opin Neurobiol* 27:179–185.
29. Ezratty EJ, Partridge MA, Gundersen GG (2005) Microtubule-induced focal adhesion disassembly is mediated by dynamin and focal adhesion kinase. *Nat Cell Biol* 7: 581–590.
30. Woo S, Rowan DJ, Gomez TM (2009) Retinotopic mapping requires focal adhesion kinase-mediated regulation of growth cone adhesion. *J Neurosci* 29:13981–13991.
31. Robles E, Gomez TM (2006) Focal adhesion kinase signaling at sites of integrin-mediated adhesion controls axon pathfinding. *Nat Neurosci* 9:1274–1283.
32. Attal N, et al. (2009) Thermal hyperalgesia as a marker of oxaliplatin neurotoxicity: A prospective quantified sensory assessment study. *Pain* 144:245–252.
33. Wilson RH, et al. (2002) Acute oxaliplatin-induced peripheral nerve hyperexcitability. *J Clin Oncol* 20:1767–1774.
34. Casals-Díaz L, Vivó M, Navarro X (2009) Nociceptive responses and spinal plastic changes of afferent C-fibers in three neuropathic pain models induced by sciatic nerve injury in the rat. *Exp Neurol* 217:84–95.
35. Bailey AL, Ribeiro-da-Silva A (2006) Transient loss of terminals from non-peptidergic nociceptive fibers in the substantia gelatinosa of spinal cord following chronic constriction injury of the sciatic nerve. *Neuroscience* 138:675–690.
36. Makker PG, et al. (2017) Characterisation of immune and neuroinflammatory changes associated with chemotherapy-induced peripheral neuropathy. *PLoS One* 12: e0170814.
37. Tarpley JW, Kohler MG, Martin WJ (2004) The behavioral and neuroanatomical effects of IB4-saporin treatment in rat models of nociceptive and neuropathic pain. *Brain Res* 1029:65–76.
38. Boucher TJ, et al. (2000) Potent analgesic effects of GDNF in neuropathic pain states. *Science* 290:124–127.
39. Dubový P (2011) Wallerian degeneration and peripheral nerve conditions for both axonal regeneration and neuropathic pain induction. *Ann Anat* 193:267–275.
40. Bradke F, Fawcett JW, Spira ME (2012) Assembly of a new growth cone after axotomy: The precursor to axon regeneration. *Nat Rev Neurosci* 13:183–193.
41. Tucker BA, Rahimtula M, Mearow KM (2008) Src and FAK are key early signalling intermediates required for neurite growth in NGF-responsive adult DRG neurons. *Cell Signal* 20:241–257.
42. D'Arcangelo G, Halegoua S (1993) A branched signaling pathway for nerve growth factor is revealed by Src-, Ras-, and Raf-mediated gene inductions. *Mol Cell Biol* 13: 3146–3155.
43. Rico B, et al. (2004) Control of axonal branching and synapse formation by focal adhesion kinase. *Nat Neurosci* 7:1059–1069.
44. Calalb MB, Polte TR, Hanks SK (1995) Tyrosine phosphorylation of focal adhesion kinase at sites in the catalytic domain regulates kinase activity: A role for Src family kinases. *Mol Cell Biol* 15:954–963.
45. Gomez TM, Letourneau PC (2014) Actin dynamics in growth cone motility and navigation. *J Neurochem* 129:221–234.
46. Turney SG, Bridgman PC (2005) Laminin stimulates and guides axonal outgrowth via growth cone myosin II activity. *Nat Neurosci* 8:717–719.
47. Lin CH, Espreafico EM, Mooseker MS, Forscher P (1996) Myosin drives retrograde F-actin flow in neuronal growth cones. *Neuron* 16:769–782.
48. Vallee RB, Seale GE, Tsai JW (2009) Emerging roles for myosin II and cytoplasmic dynein in migrating neurons and growth cones. *Trends Cell Biol* 19:347–355.
49. Luo L (2002) Actin cytoskeleton regulation in neuronal morphogenesis and structural plasticity. *Annu Rev Cell Dev Biol* 18:601–635.
50. Turney SG, et al. (2016) Nerve growth factor stimulates axon outgrowth through negative regulation of growth cone actomyosin restraint of microtubule advance. *Mol Biol Cell* 27:500–517.
51. Sydor AM, Su AL, Wang FS, Xu A, Jay DG (1996) Talin and vinculin play distinct roles in filopodial motility in the neuronal growth cone. *J Cell Biol* 134:1197–1207.
52. Chen K, Zhang W, Chen J, Li S, Guo G (2013) Rho-associated protein kinase modulates neurite extension by regulating microtubule remodeling and vinculin distribution. *Neural Regen Res* 8:3027–3035.
53. Coleman MP (2013) The challenges of axon survival: Introduction to the special issue on axonal degeneration. *Exp Neurol* 246:1–5.
54. Xiao WH, Zheng H, Bennett GJ (2012) Characterization of oxaliplatin-induced chronic painful peripheral neuropathy in the rat and comparison with the neuropathy induced by paclitaxel. *Neuroscience* 203:194–206.
55. Detloff MR, Smith EJ, Quiros Molina A, Ganzer PD, Houllé JD (2014) Acute exercise prevents the development of neuropathic pain and the sprouting of non-peptidergic (GDNF- and artemin-responsive) c-fibers after spinal cord injury. *Exp Neurol* 255: 38–48.
56. National Research Council of the National Academies (2011) *Guide for the Care and Use of Laboratory Animals* (National Academies Press, Washington, DC), 8th Ed.
57. Cheng CM, et al. (2010) Probing localized neural mechanotransduction through surface-modified elastomeric matrices and electrophysiology. *Nat Protoc* 5:714–724.
58. Dib-Hajj SD, et al. (2009) Transfection of rat or mouse neurons by biolistics or electroporation. *Nat Protoc* 4:1118–1126.
59. Toyama S, et al. (2014) Characterization of acute and chronic neuropathies induced by oxaliplatin in mice and differential effects of a novel mitochondria-targeted antioxidant on the neuropathies. *Anesthesiology* 120:459–473.
60. Lin CC, et al. (2012) An antinociceptive role for substance P in acid-induced chronic muscle pain. *Proc Natl Acad Sci USA* 109:E76–E83.
61. Bonin RP, Bories C, De Koninck Y (2014) A simplified up-down method (SUDO) for measuring mechanical nociception in rodents using von Frey filaments. *Mol Pain* 10: 26.
62. Liu L, Duff K (2008) A technique for serial collection of cerebrospinal fluid from the cisterna magna in mouse. *J Vis Exp* 21:e960.